



Untangling electronic, optical and bonding properties of hexagonal bismuth borate $\text{SrBi}_2\text{B}_2\text{O}_7$ crystal for ultraviolet opto-electronic applications: An ab initio study



Naouel Boudghene Stambouli ^{a, b, **, *}, Tarik Ouahrani ^{a, b, *}, Michael Badawi ^c,
Ali H. Reshak ^{d, e, f}, Sihem Azizi ^b

^a École Supérieure en Sciences Appliquées, B.P. 165, Tlemcen, 13000, Algeria

^b Laboratoire de Physique Théorique, Université de Tlemcen, 13000, Algeria

^c Université de Lorraine and CNRS, LPCT, UMR 7019, 54506, Vandoeuvre-lès-Nancy, France

^d Department of Instrumentation and Control Engineering, Faculty of Mechanical Engineering, CTU in Prague, Technicka 4, 166 07, Prague 6, Czech Republic

^e Nanotechnology and Catalysis Research Center (NANOCAT), University of Malaya, Kuala Lumpur, 50603, Malaysia

^f Iraq University College (IUC), Al-Estiqal St., Basrah, Iraq

ARTICLE INFO

Article history:

Received 23 May 2019

Received in revised form

26 June 2019

Accepted 27 June 2019

Available online 29 June 2019

Keywords:

ab initio calculation

Band structure

Bonding analysis

Linear and non linear optical properties

ABSTRACT

To realize the efficient frequency conversion, the nonlinear ultraviolet crystal must exhibit strong second harmonic generation and possible phase-matching condition. The current first principles calculations predict that $\text{SrBi}_2\text{B}_2\text{O}_7$ represents potentially a new class of materials with such characteristics. For this aim, we present the first analysis of dynamical, bonding, linear and nonlinear optical properties of the $\text{SrBi}_2\text{B}_2\text{O}_7$ single crystal. To untangle such properties, both density functional theory calculation and topological analysis were used. It is found that the compound exhibits a wide indirect band gap and an interesting bonding motif. In particular, the distortion caused by the stereochemically active lone pair of the s -state in the Bi^{3+} unit favors the enhancement of local dipole moment. In addition, the refraction index, absorption spectrum, phase matching and second harmonic properties were calculated and analyzed. According to the results, $\text{SrBi}_2\text{B}_2\text{O}_7$ has a large d_{33} s -order susceptibility component which makes it a very promising UV nonlinear optical material.

© 2019 Elsevier B.V. All rights reserved.

1. Introduction

To date, the wide range of applications showed by borate-based materials make them the subject of extensive and active research, either on the theoretical or experimental side [1–14]. The reason behind this interest is closely related to the inherent nature of these materials, as well as to their exceptional chemical properties [15–17]. In fact, according to the studies [8–10] done by means of the principle of anionic group theory [18], this family of materials has many advantages. Indeed, due to the large difference in the electronegativities of the elements in B–O bond, these materials

are transparent far into the UV and even deep-UV regions. In addition, such compounds crystallize in hundreds of different structures, which opens a large opportunity to synthesize them. From a crystal chemistry point of view, in such structures, boron atoms do occur equiprobably in both triangular and tetrahedral coordination to oxygen atoms and hydroxyl groups in the structures of crystals and glasses [11], that generates changes in chemical behavior of the crystal and many interesting optical properties. Concerning practical application, the intrinsic damage threshold in these crystals is very high on account of the wide band gap in the electronic structure. Furthermore, they are excellent for frequency conversion of the laser beam [11]. In addition to good chemical and mechanical stability, borate materials have a wide transparency range [11,19,20]. Among borate materials, one can point the transparent multi-functional crystallized glasses, which are extensively used in optoelectronics, optical telecommunication networks [21], photonic devices, such as optical gratings and waveguides, and laser systems [22]. Using a laser-induced crystallization technique

* Corresponding author. École Supérieure en Sciences Appliquées, B.P. 165, Tlemcen, 13000, Algeria.

** Corresponding author. , École Supérieure en Sciences Appliquées, B.P. 165, Tlemcen, 13000, Algeria.

E-mail addresses: bendimered_naouel@yahoo.fr (N.B. Stambouli), touahrani@essa-tlemcen.dz (T. Ouahrani).

and a solid-state reaction route, many borates materials as $\text{ZnBi}_2\text{B}_2\text{O}_7$ [23], $\text{CaBi}_2\text{B}_2\text{O}_7$ [24] and $\text{SrBi}_2\text{B}_2\text{O}_7$ [25] have been patterned successfully into transparent glasses [26]. These experimental studies propose to use these materials in UV and deep-UV regions. The same experiments [23–25] reveal that these materials have a variety of merits to be employed in nonlinear optics field due to its significant second harmonic generation properties. In particular, their wide spectral transmission and phase-matching range are obviously fundamental properties for application in laser field, especially in the deep-UV, far IR, and even THz spectral regions. By doping borate materials/glasses with rare earth elements, one can modify their optical properties. For instance, when being doped with rare earth ions, the $\text{SrBi}_2\text{B}_2\text{O}_7$ shows interesting luminescence and thermal stability [27]. $\text{SrBi}_2\text{B}_2\text{O}_7$ structure contains SrO_6 trigonal prisms which makes it to be appropriate host [27] for big cations. Also, good orange-red emissions were showed by doping it with Eu^{3+} cations [28]. Furthermore, it can also generate intense reddish light combined with the Sm^{3+} cations [27].

From a fundamental point of view, the molecular organization of $\text{ZnBi}_2\text{B}_2\text{O}_7$, $\text{CaBi}_2\text{B}_2\text{O}_7$ and $\text{SrBi}_2\text{B}_2\text{O}_7$ compounds is quite interesting. Indeed, the structure is composed of corner-sharing BO_3 triangles as the central building where the B–O polyanions are repeated [29]. These structural characteristics confer to $\text{SrBi}_2\text{B}_2\text{O}_7$ the highest degree of B–O polyhedral polymerization [30]. Surplus, the Bi^{3+} contains a lone stereo-active electron pair, leading to a structural distortion of a d^0 cation with a second-order Jahn-Teller type effect [31–33].

Given that, the search of wide gap borate crystals is of great importance for UV-NLO applications. Knowing the bonding, as well as a deeper electronic analysis for the title compound is essential. Using first principle calculation as well as topological analysis of the electron density [35], the authors of the paper [34] took a special point of view to investigate dipole and quadrupole moments of the $\text{CaBi}_2\text{B}_2\text{O}_7$ and $\text{ZnBi}_2\text{B}_2\text{O}_7$ single crystals. In this study, the B_2O_5 anionic group was studied by means of the Bader theory of atoms in molecules [35]. Special attention pointed out the asymmetric bonds and the anisotropy of the atomic basin of this unit. To the best of our knowledge, no detailed investigation of the $\text{SrBi}_2\text{B}_2\text{O}_7$ compound was reported in the literature. Therefore, it would be worthwhile to perform theoretical calculations in order to achieve a coherent analysis of bonding, linear and nonlinear optical properties of this compound. As an efficient route to obtain energy band gap value, the mBJ exchange-correlation potential [36] is employed. Recent works have highlighted the ability of this computationally cheap functional to predict quite accurately band gaps of InSe or GaSe systems in comparison with experiment [37,38] or more sophisticated methods such as HSE or mBJ [38].

In the next section a brief description of the computational background used in this study is given. We then gather our main results based on density functional calculations in section 3. In the first part of this section, we will deal with the structural, elastic, electronic and chemical bonding properties of $\text{SrBi}_2\text{B}_2\text{O}_7$. In the second part, the linear and nonlinear optical properties are presented for $\text{SrBi}_2\text{B}_2\text{O}_7$ material. Our mains conclusion are given in section 4.

2. Computational method

The calculations in the framework of the density functional theory (DFT) scheme were carried out within the FP-LAPW_{ELK} package [39]. To discretize the Brillouin zone, a $8 \times 8 \times 5$ \mathbf{k} -points grid has been used. In addition, based on our convergence tests, the parameter $R_{\text{min}} \times G_{\text{max}}$ was taken equal to 8, Fourier expanded charge density was truncated at $G_{\text{max}} = 12$, and the empty states equal to 50. The atomic positions are relaxed until all the forces

were below a threshold of $F_{\text{tol}} = 1.00$ mRy/atom. Furthermore, to evaluate the reliability of our results, two different exchange-correlations functional were used, namely, the local-density approximation (LDA) [40] and the generalized-gradient approximation via the Perdew-Burke-Ernzerhof approximation (GGA-PBE) [41]. Thus, to ensure the accuracy of the ground-state calculations of the investigated structure, a full structural optimization was performed. The modified Becke and Johnson (mBJ) [36] and EngelVosko-GGA (EV-GGA) formalisms [42] were used to compute the optoelectronic properties. Moreover, using filled band, the random phase approximation (RPA) [43] were treated to analyze the optical response of $\text{SrBi}_2\text{B}_2\text{O}_7$. A dense mesh of uniformly distributed \mathbf{k} -points (800 \mathbf{k} -points) was used. In this manner, a purely interband contribution was calculated, and dense eigenvalues and momentum matrix element were needed [44].

For practical purposes, the topology of electronic density (ρ) and the electron localization function (ELF) [45] were analyzed within the quantum theory of atoms in molecule QTAIM [35] implemented in the **critic** code [46]. In these two procedures, the electronic domains are divided into additive atomic contributions that could be labeled as basins (Ω) [35,47]. These basins have well-defined boundaries and encompass a finite volume [35]. In each of these domains, maximums and attractors are assimilated to a number of critical points labeled (CP). These ones emerge from the condition of zero flux of the gradient of the electron density: $\nabla\rho(\mathbf{r}) \cdot \mathbf{n}(\mathbf{r}) = 0$ [35]. The integration of atomic properties inside the basins (Ω) gives detailed pieces of information about the chemical bonding of material.

3. Results and discussion

3.1. Structural and elastic properties

By means of melt-quenching technique, it was shown in experiments that $\text{SrBi}_2\text{B}_2\text{O}_7$ nanocrystals can be patterned in $\text{SrO-Bi}_2\text{O}_3\text{-B}_2\text{O}_3$ (SBBO) glasses and they can be crystallized in different orientations [26]. Barbier and Cranswick [48] synthesized the $\text{SrBi}_2\text{B}_2\text{O}_7$ crystal and analyzed it using the neutron diffraction technique. They found that the compound crystallizes in P6_3 polar space group without c-glide symmetry. Another experiment to grow this material by crystallization from glass ceramics for a stoichiometric $\text{Sr}_{1-x}\text{Ba}_x\text{Bi}_2\text{B}_2\text{O}_7$ solution was recently done in Refs. [27,29]. Both works present a detailed description of the structure and confirm that the material can be crystallized in the hexagonal P6_3 phase. The non-centrosymmetric single crystals structure of the title compound is built from a stacking of stoichiometric layers in the \mathbf{c} direction (see Fig. 1). The BO_3 triangles and SrO_6 trigonal prisms are shared by corner. In the same time, the Bi atoms are bonded to the O atoms of the SrO_6 groups. The BO_3 triangle is also connected to BiO_3 ones via common corners. In this manner, BO_3 units form a rigid cyclic 3B-groups. Long and weak Bi–O bonds can be also identified between the adjacent layers parallel to the \mathbf{c} direction. In addition to these units, the compound contains seven-fold coordinated Sr^{2+} (6c) sites, eight-fold coordinated Bi(1) (6c) sites, and eight-fold coordinated Bi(2) (6c) sites [48].

A large number of parameters are involved in the energy minimization, such as the lattice parameter a and c , the c/a ratio and many internal atomic positions, which demand several total energy calculations. The calculation of bulk modulus (B_0) also required a full optimization for selected volumes around the experimental one. The optimized results are summarized in Table 1. Generally, the structural parameters are in good agreement with the available experimental data. As expected, the calculations within PBE-GGA exchange-correlation functional scheme give an

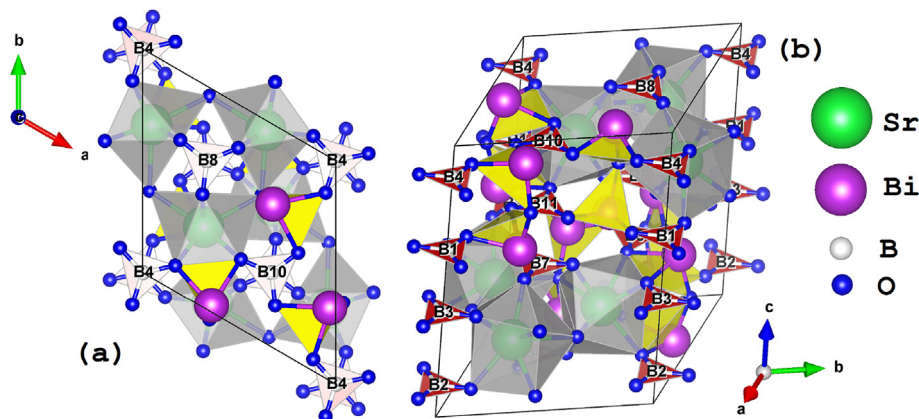


Fig. 1. Crystal structure of $\text{SrBi}_2\text{B}_2\text{O}_7$ space group $P6_3$, shown in in two orientations. Here, the SrO_6 , BO_3 and BiO_3 polyhedral units are respectively colored in gray, red and yellow. (For interpretation of the references to color in this figure legend, the reader is referred to the Web version of this article.)

Table 1

Calculated lattice parameters, bulk modulus, and volumes at LDA and PBE-GGA levels of the $\text{SrBi}_2\text{B}_2\text{O}_7$ compound.

	GGA-PBE	LDA	experiment/averaged value
$a(\text{\AA})$	9.229, 9.222 ^a	8.999	9.140/9.114
$c(\text{\AA})$	13.237, 13.249 ^a	12.706	13.080/12.972
Volume(\AA^3)	976.889, 975.911 ^a	891.259	946.44/934.074
Bulk (GPa)	46.596	57.557	-

^a Calculated from an unpublished work of Materials Project database [49].

overestimation of lattice constant, which are, however, similar to *Materials Project database* [49]. Thus, in order to approach the experimental evidence within an averaged value (i.e $(GGA) + (LDA)/2$), some calculations at the LDA level were carried out for the sake of comparison with GGA results. It is seen from results gathered in *Table 1*, that averaged value is very close to the experimental one of Barbier *et al.* [48], which confirms the consistency of our calculations.

In order to analyze the stability of the $\text{SrBi}_2\text{B}_2\text{O}_7$ structure, the elastic tensor was determined by performing appropriate finite distortions of the lattice parameters and deriving the elastic constants from the strain-stress relationship [50]. The results are gathered in *Table 2*. In a survey of the dynamical properties of $\text{SrBi}_2\text{B}_2\text{O}_7$, we found no experimental report or theoretical results for elastic constants. Therefore, we can consider the present computational study as predictive. However, in any case, the mechanical stability conditions ($C_{44} > 0, C_{11} - C_{12} > 0, C_{33}(C_{11} + C_{12}) - 2C_{13}^2 > 0$) for hexagonal crystals at 0 GPa are satisfied. The small value of C_{44} from *Table 2* indicates that the compound is very sensitive to shear deformation [52]. Additionally, the C_{11} is found greater than the C_{33} one, manifesting that the bond strengths along the [100] and [010] directions are much stronger than that in the [001] direction, see for example Refs. [53,54]. On the base of predicted elastic constants, we derived the bulk B , Young Y and shear modulus G from the Voigt-Reuss-Hill approximation [51], as well as the other related

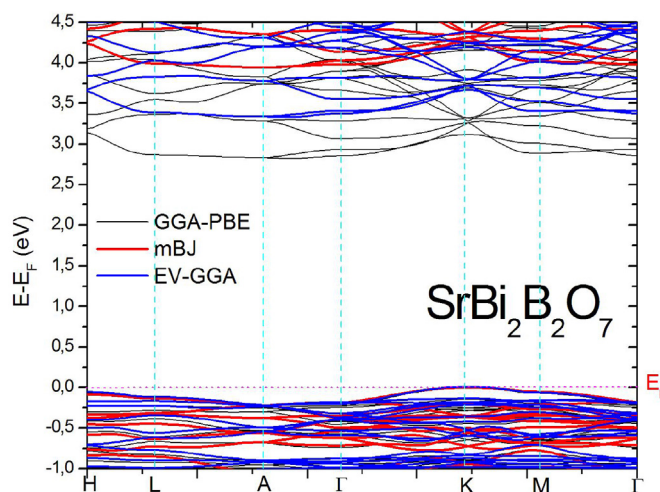


Fig. 2. Band structures of $\text{SrBi}_2\text{B}_2\text{O}_7$ calculated via GGA-PBE, mBJ and EV-GGA.

quantities [55,56](i.e Poisson's ratio σ and Lamé coefficient λ), all displayed in *Table 2*. These results indicate clearly the weak ability of the investigated compound to resist to the volume deformation. Also, some selected thermal quantities as Debye temperature (Θ_D) volume and pressure constant heat capacities ($C_{v,p}$) are given in the same table. Consequently, the present computed elastic properties allow us to stipulate that $\text{SrBi}_2\text{B}_2\text{O}_7$ has a brittle character.

3.2. Electronic properties

The clarification of the electronic structure of the $\text{SrBi}_2\text{B}_2\text{O}_7$ compound is mandatory if we look for the analysis of optical spectra which is directly derived from the inter-electronic state transitions. In this respect, we calculated the band structure of

Table 2

Calculated elastic constants (C_{ij} in GPa) for the $\text{SrBi}_2\text{B}_2\text{O}_7$ compound (C_{66} is equal to $(C_{11} - C_{12})/2$). From them a polycrystalline material (GPa) are calculated, like Bulk (B), shear (G) modulus in Voigt (V), Reuss (R) and Hill (H) approximation given in GPa unite. Additionally, elastic Debye temperature (Θ_D) (K), averaged sound velocity (v_t) (m/s), Lamé coefficient λ , Young modulus (Y) in GPa and volume (C_v) and pressure (C_p) constant heat capacities are also given in ($\text{J}\cdot\text{mol}^{-1}\cdot\text{K}^{-1}$) unite.

C_{11}	C_{12}	C_{13}	C_{33}	C_{44}	C_{66}	B	B_R	B_V	B_H	G_R	G_V	G_H
125.003	52.567	15.899	61.633	1.168	49.718	44 ± 3.659	44.0	53.37	48.687	22.862	2.781	12.822
53.374	44.0	48.687	0.312	0.469	0.378	38.132	42.146	35.360	48.633	49.153	134.373	1077.273
		Y_H	σ_V	σ_R	σ_H	λ_V	λ_R	λ_H	C_V	C_P	Θ_D	v_t

SrBi₂B₂O₇ using three approximations: the GGA-PBE, EV-GGA approaches, and the mBJ potential. The plot of band structure at the first Brillouin zone is displayed in Fig. 2. It is noticed that the valence bands are very flat, and the conduction bands have some oscillations. The lowest energy of the conduction bands is located at the point between *L* and *A*, whereas the highest energy of the valence bands is located at the *K* point, as shown in Fig. 2; hence, SrBi₂B₂O₇ has an indirect band gap. Our calculated band gap values (E_g) within GGA, EV-GGA and mBJ approaches are respectively 2.812, 3.34 and 3.94 eV. It is unfortunate that no theoretical result has been reported until now for band gap value. The only value of $E_g = 2.804$ eV was found the Materials Project database [49], where the value was obtained at the GGA level using the projector-augmented wave (PAW) and plane waves basis set scheme implemented in the Vienna ab initio simulation package (VASP) [57]. The wide bandgap in SrBi₂B₂O₇ will assure its utilization as a high-power w-LEDs [27]. In order to view the energetic contribution of each orbital, the partial densities of states at mBJ level are plotted, as illustrated in Fig. 3. To correctly analyze these plots, we begin by estimating the Mulliken population of each orbital. On one hand, the electronic configuration of O ($2s^2 2p^4$) gives a Mulliken population of 0.54e and 1.61e for the *s* and *p* orbitals, respectively. The electronic population of Bi ($5d^{10} 6s^2 6p^3$) was estimated by 1.84e for *s*, 1.52e for *p* and 10.00e for the *d* orbitals. The Sr ($4s^2 4p^6 5s^2$) one has, on the other hand, 2.25e for *s*, 6.00e for *p* and 0.57e for the *d* state. The Boron (B) atom of a $2s^2 2p^1$ configuration, has 0.54e and 1.61e for, respectively, *s* and *p* orbitals. According to Fig. 3, the O-*p* states are distributed energetically near the Fermi level, in the range of -6 to 0 eV, (noted that in Fig. 3, the Fermi level is adjusted to zero eV). The *s* and *p* states of the Bi atoms have also the same energetic distribution than those of oxygen. However, the intensity of electronic states of O atoms is much stronger than that of Bi atoms. We note also that the upper occupied states involve strong unoccupied Bi-6*s*, 6*p* and O-2*p* orbitals. The fact that Bi-6*s* states have a contribution in valence band maximum thought about the existence of stereochemically active lone pair effect. The Bi-6*s* and Bi-6*p* orbitals occupied the same state than the O-2*p* ones within a strong hybridization. Also, the Bi–O interactions are dominant at the bottom part of the conduction band. The energy range from -23.5 eV to 18 eV, located far from the Fermi surface is composed by all the Bi-5*d* orbitals, the most O-2*s* orbitals and a small part of B-2*s*2*p* mixed with the Bi-6*s*6*p* ones. Finally, the plot of partial densities of states shows also a non negligible part on Bi-6*s* orbital occupying the energy range between -10 and -8 eV. The

electronic structure and PDOS analysis show that the optical absorption around the Fermi level is mainly occurring from occupied O-2*p* with Bi-*sp*/Sr-*d* to unoccupied Bi-6*p*/B-2*p* and O-2*p* states.

3.3. Bonding properties

As it is mentioned below, SrBi₂B₂O₇ is a non-centrosymmetric crystal that makes it a candidate for a wide and diverse range of optical applications. Therefore, it is topical to analyze its chemical character. To this end, we have used a topological analysis of the electronic density. The purpose of this procedure is to grasp and identify the electronic behavior of each bond and atoms controlling the optical properties of the SrBi₂B₂O₇ compound. For this aim, we have used the **critic** code [46], which implements a topological procedure based on the atoms in molecule theory (AIM) [35] as well as the Electron Localization Function (ELF) index [45]. In these approaches, the gradient fields and space partitioning define the two most common operation modes, where densities are integrated over the 3D basins. A fine FFT grid was used to reproduce the correct total charge. To show the participation of each electronic orbital toward the optical response of the SrBi₂B₂O₇ single crystal, we begin by integrating the effective charge and atomic volumes of each basin, the results are gathered in Table 3. These quantities are of paramount importance to entirely figure out the charge transfer, the polarizabilities, and the electronegativity influence. By calculating the ratio between topological charges $\mathcal{C}(\Omega)$ and nominal oxidation states $OS(\Omega)$, we have estimated the *degree of ionicity* by the following formula $\alpha = \frac{1}{N} \sum_{\Omega=1}^N \frac{\mathcal{C}(\Omega)}{OS(\Omega)}$ (A more elaborate discussion on the performance of this index is given in Ref. [58]). α gives a value of 57.56%. This means that the compound has a dominant covalent character, but also mixed with some ionicity one. As a qualitative check of Table 3, one can note that the oxygen anions, which have a multiplicity equal to six, have 50% of charges transfer; however, those with a multiplicity of 12, are more transferred. This is because they are almost linked with the BO₃ units. In fact, owing to the electron affinity of the oxygen atom, it causes certain polarizability in the BO₃ triangle. The situation is more pronounced with respect to the Sr and Bi cations, the charge transfer along the Sr–O and Bi–O bonds in the same plane of the BO₃ units, can largely influence the value of microscopic susceptibility.

One can gain some insight into the bonding analysis by exploring the derivative of electronic density (ρ). Thus, in order to provide a further assessment in this task, we also used the electron localization function (ELF) to grasp the electronic affinity of each bond. However, before to make this task, let us carry out a rapid bond length analysis. It is found that the B–O bonds forming the rigid cyclic 3B-groups are almost equal (~ 1.38 Å), whereas, the Bi–O ones forming the BiO₃ units have not similar length (2.17 Å, 2.26 Å, and 2.32 Å), that results in a considerably asymmetric BiO₃ polyhedral [63].

Table 3

Calculated effective charges ($q(\Omega)$) and its related volume ($V(\Omega)$), $\mathcal{C}\mathcal{F}(\Omega) = 1 - (OS(\Omega) - \mathcal{C}(\Omega))/OS(\Omega)$, and mult represent respectively the charge transfer and the multiplicity of the atoms.

atom	mult	$V(\Omega)$ (a.u.)	$q(\Omega)$ (electron)	$\mathcal{C}\mathcal{F}(\Omega)$
B	4	12.76	2.28	76.13%
B	4	12.99	2.33	77.82%
B	4	11.35	2.34	78.00%
Bi	12	130.96	1.19	39.50%
O	12	102.67	-1.47	73.39%
O	12	92.78	-1.41	70.50%
O	12	100.80	-1.49	74.50%
O	6	103.85	-1.17	58.50%
Sr	6	115.74	1.69	84.50%

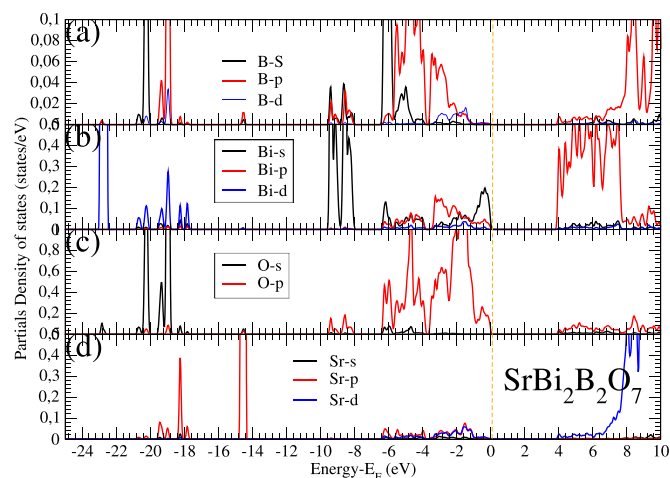


Fig. 3. Partial densities of states of the SrBi₂B₂O₇ compound. (a), (b), (c) and (d) plots represent the contribution of respectively B, Bi, O, and Sr atoms.

The ELF topology is presented in Fig. 4. The plot clearly reveals that the electronic domain along the BiO_3 and BO_3 is different. The B–O bonds are clearly covalent. Consequently, based on the anionic group theory [59,60], the contribution of the BO_3 triangles in the second order susceptibility is not negligible. In addition, all cation-centered polyhedra are polar and show spherical ELF isosurface, which leads probably to a nonzero static dipole moment along Bi–O and Sr–O bonds. These two ELF attractors are equal, respectively, to 0.60 and 0.85, while the attractors between the O and B atoms have a value of 0.88. Three other attractors are also distinguished in Fig. 4: one centralized on the lone pair (LP) around the oxygen linked to the B–O bond, and two other close to the Bi and Sr cations. The attractor of the LP basin close to the Bi cation seems to have low ELF value of 0.60. The electronic population of the B–O, Bi–O and Sr–O bonds are equal, respectively, to 0.80, 0.28 and 0.14 electron. However, the LP around the Bi one has a population equal to 0.05 electrons. This latter is, in fact, the attractor of a stereochemically active lone-pair basin (see the attractors colored in red in Fig. 4). This attractor occurs because of the difference in size and electron structure between the Bi cation and the O anion. Here, the lone pair affects its surrounding oxygen atoms and leads to a large bond angle of O–Bi–O. This means that the $6s^2$ LP around the Bi cation is structurally active and the Bi^{3+} ions generate distorted structures due to the electrostatic effect of the lone pair of electrons. In order to understand the origins of permanent and induced molecular dipole moments and dielectric polarization in the title compound, we have estimated dipolar polarization quantities ($|\mu| = \sqrt{\mu_x^2 + \mu_y^2 + \mu_z^2}$) [61–63] related to each ion. The results in (a.u) unit give $|\mu_{\text{Sr}}| = \sqrt{(-0.02)^2 + (0.02)^2 + (0.00)^2}$, $|\mu_{\text{Bi}}| = \sqrt{(0.22)^2 + (-0.27)^2 + (-0.55)^2}$ and $|\mu_{\text{O}}| = \sqrt{(-0.21)^2 + (0.94)^2 + (0.03)^2}$. The results are correlated to the calculated charge transfer in the last paragraph as well as with the density distributions in each ion. The group contributions of the electric polarizability ($|\mathcal{C}| = \sqrt{\frac{2}{3}(\mathcal{C}_{xx}^2 + \mathcal{C}_{yy}^2 + \mathcal{C}_{zz}^2)}$) [35] of the BiO_3 and SrO_6 units were calculated and found equal respectively to 5.63 (a.u) and 10.73 (a.u) (It is to note that $|\mathcal{C}(\text{Sr})| = 0.17$ (a.u), $|\mathcal{C}(\text{Bi})| = 0.35$ (a.u) and $|\mathcal{C}(\text{O})| = 1.76$ (a.u)). Both dipole and quadrupole moments calculation shown that the BiO_3 is the more involved in the optical properties.

3.4. Optical properties

Since the optical properties of a solid do not depend only to the bonding character, but also on its electronic properties due to electronic excitation in crystals upon incidence of the electromagnetic wave, it is mandatory to explore the macroscopic quantities related to the dielectric function. For this aim, interband and intraband energetic transitions connected to band structure coming from mBJ(EV-GGA) calculations were used to investigate linear and nonlinear properties. The results from GGA-PBE are also shown for comparison but not analyzed due to their underestimation of the band gap value. The knowledge of optical properties like UV absorption spectra can assess the improved physical resources of the fabricated UV sensor. This task is essential in measuring the intensity of UV radiation in a convenient way. The absorption spectra is calculated following the formula: $I(\omega) = \frac{2\omega}{c} \sqrt{(1/2 \times (\varepsilon_1^2(\omega) + \varepsilon_2^2(\omega))^{1/2}) - \varepsilon_1(\omega) \cdot \varepsilon(\omega)}$ being the macroscopic dielectric function evaluated from permitted transitions, i.e., the intra- and inter-band contributions (the indexing by 1 and 2 indicates respectively the real and imaginary parts of the dielectric function) and c is the speed of light in vacuum. These measures depend on the momentum matrix elements [43] and originate from the charge transfer of valence electrons to the conduction bands. The electrons from these bands can, in fact, redistribute the charge density and adjust the dipole moment considerably.

The absorption spectra are displayed in Fig. 5, where one can see that the crystal exhibits high transparency in the UV portion of the spectrum, opening a wide window for UV applications. It is observed that a sharp edge of the $I(\omega)$ spectra starts at the absorption edge of ~ 315 nm close to the near-UV spectral region. The curve shows also a particular energy range in the middle and deep UV ones with small oscillations at higher energies. The maximum absorption is reached for the Vacuum UV range. However, the first absorption valley is rather situated in the deep UV range, where its most important peaks depend upon the quantitative contribution of inter-band/or intra-band transitions from Bi-s to O-p orbitals. Another route to explore the transparency of the material is to analyze the refractive index spectrum. Such quantity is calculated according to formula: $n(\omega) = \sqrt{(1/2) \times \{(\varepsilon_1^2(\omega) + \varepsilon_2^2(\omega))^{1/2} + \varepsilon_1(\omega)\}}$. The dispersive refractive indices are plotted in Fig. 6(a). In our uniaxial material, the unique optic axis is along with the highest C_6 symmetry axis. In this hexagonal crystal, the light beam is conventionally splitted into

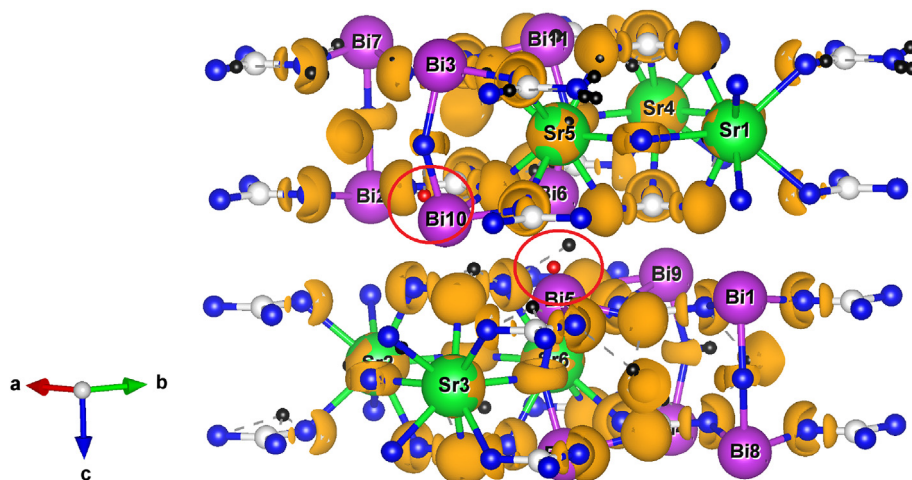


Fig. 4. ELF localization domains (ELF = 0.84) of the $\text{SrBi}_2\text{B}_2\text{O}_7$ compound. The stereochemically active lone-pair attractors are circled in red. The small black balls show disynaptic and monosynaptic attractors. (For interpretation of the references to color in this figure legend, the reader is referred to the Web version of this article.)

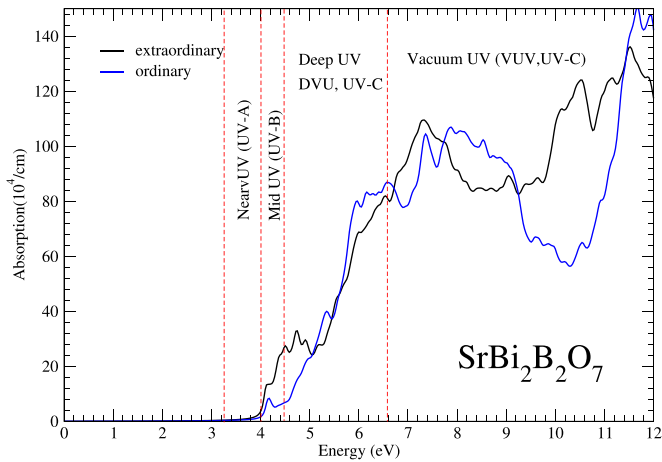


Fig. 5. The absorption spectra of the SrBi₂B₂O₇ compound.

ordinary (*o*) and extraordinary (*e*) ones. The static value of the refractive indices ($n(0)$) and mBJ(EV-GGA) levels are found to be 1.719(1.963) and 1.783(1.845), respectively, for the extraordinary and ordinary components. The small value of refractive index explains the transparency of the title compound. Another important characteristic is found in the strong anisotropy between the $n_o(\omega)$ and the $n_e(\omega)$ spectra. It is worth noting that the strong anisotropy of $n(\omega)$ spectra favors the SrBi₂B₂O₇ compound to produce a deep-UV harmonic generation. Conventionally, the birefringence is defined as $\Delta n = (n_e - n_o)$. We can clearly extract from the plot of refractive index in Fig. 6 the values of $\Delta n = -0.085(0.153)$ @532 nm and $\Delta n = -0.08(0.109)$ @1064 nm for 2ω and ω frequencies. These values are comparable to the measured birefringence of the widely used β -BaB₂O₄ nonlinear compound [64,65]. Accordingly, the title compound belongs to a family of a negative uniaxial crystal. We have calculated the value of $n_o(\omega) = 1.78$ and found it in concordance with that of $n_e(2\omega) \approx 1.77$, which stipulates that SrBi₂B₂O₇ is a type I phase-matching material [66], see Fig. 6(b). Moreover, the condition $\Delta k = k(2\omega) - k(\omega) = \left(\frac{4\pi}{\lambda} [n(2\omega) - n(\omega)]\right)$ of phase-matching is achieved for this compound, which makes it suitable for the SHG process. For this material, the response of two ordinary

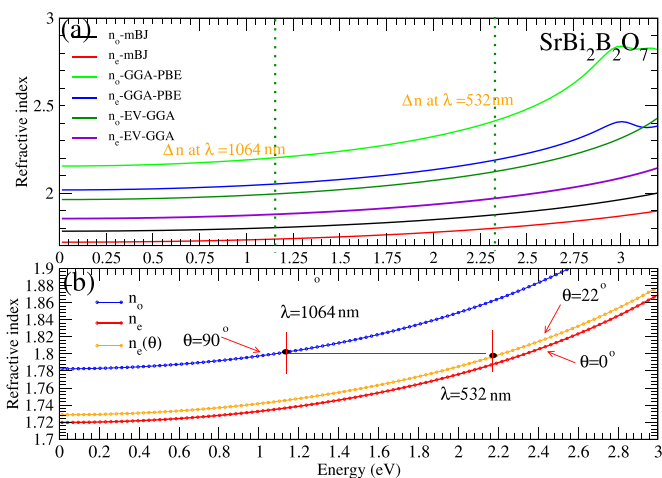


Fig. 6. (a) Refractive index at three XC levels (Δn is calculated at both @1064 nm and @532 nm frequencies), and (b) the phase matching condition ($o(\omega) + o(\omega) \rightarrow e(2\omega)$) plot of the SrBi₂B₂O₇ compound.

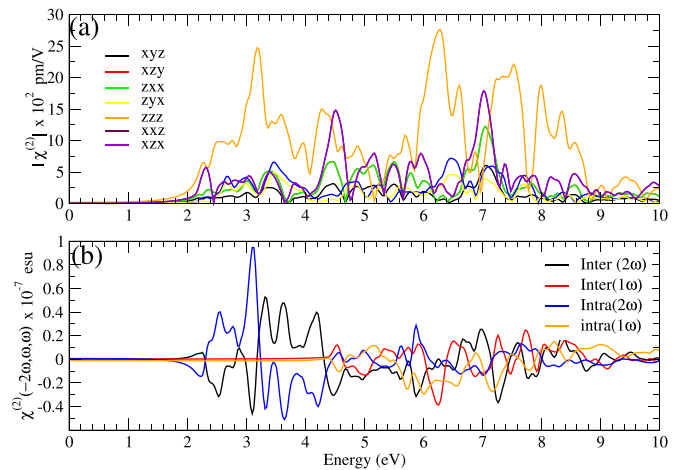


Fig. 7. (a) The magnitude of the seven non zero components of the SrBi₂B₂O₇ compound in pm/V unit. (b) Calculated total and imaginary parts of the $\chi_{zzz}^{(2)}$ spectrum as well as the intra- $2\omega/\omega$ - and inter- $2\omega/\omega$ -band contributions. All $(\text{Im}) \chi^{(2)}$ values are multiplied by 10^{-7} in esu unit.

waves at the fundamental wavelength combine to produce an extraordinary wave at the second-harmonic, $o(\omega) + o(\omega) \rightarrow e(2\omega)$. The birefringence phase matching can be employed for generating DUV lights and short wavelengths. In addition, the phase matching condition for frequency doubling can be achieved by rotating the crystal by an angle (Θ_{pm}) equal to a value given by the formula [66]: $1/n_{e,2\omega}^2(\Theta_{pm}) = \sin^2(\Theta_{pm})/n_{e,2\omega}^2 + \cos^2(\Theta_{pm})/n_{o,2\omega}^2$ to 21.988° .

Deep-ultraviolet nonlinear optical (NLO) materials can produce coherent ultraviolet (UV) light through laser frequency conversion. Thus, as an important trend to analyze in this contribution, is the nonlinear optical response of the SrBi₂B₂O₇ compound. For this task, we have calculated the second harmonic generation effect by evaluating the $\chi_{ijk}^{(2)}$ coefficients. Second harmonic generation (SHG) effect is a nonlinear optical process in which a material interacts with an incident electric field in such a way that the frequency of incoming photons is doubled by the presence of the material. The SrBi₂B₂O₇ material has a space group number #173, (P6₃) with C₆ symmetry. Thus, according to Kleinman symmetry conditions [67], and other symmetries governing the susceptibility tensors [68], the corresponding nonzero $\chi^{(2)}$ components are $xyz = -yxz$, $zxy = -yzx$, $xzx = yzy$, $xxx = yyz$, $zxx = zyy$, zzz , $zxy = -zyx$. The calculation of the absolute value of $|\chi^{(2)}|$ shown in Fig. 7(a), reveals that the $|\chi_{zzz}^{(2)}|$ is the dominant SHG component. This result is comparable with what is already found for both orthorhombic ZnBi₂B₂O₇ and CaBi₂B₂O₇ compounds in Ref. [34]. Additionally, to have more information about the one (ω)- and/or two-photon (2ω) resonances involved in the excitation leading to the SHG response; the contributions of both ω and 2ω terms are presented in Fig. 7(b). It is shown that the contributions of interband $2\omega+1\omega$ resonances have an opposite sign of inter and intraband $2\omega+1\omega$ ones, this trend gives to the fulfillment of the phase matching condition. The absolute values of dominant susceptibilities are represented in Fig. 8. As can be seen, many peaks appeared and the maximum values of nonlinear response are located around 2.32, 2.55, 3.14 and 3.58 eV below the band gap energy, as originates from the intra-bands 2ω contributions. Also, a large peak observed at 4.28 eV is mainly due to the imaginary part of the 2ω two-photon (2ω) inter-band component. The intra-bands resonance becomes significant at large photon energies (5.69 and 7.72 eV), but the 2ω component is canceled out by the ω components. The high-energy nonlinear

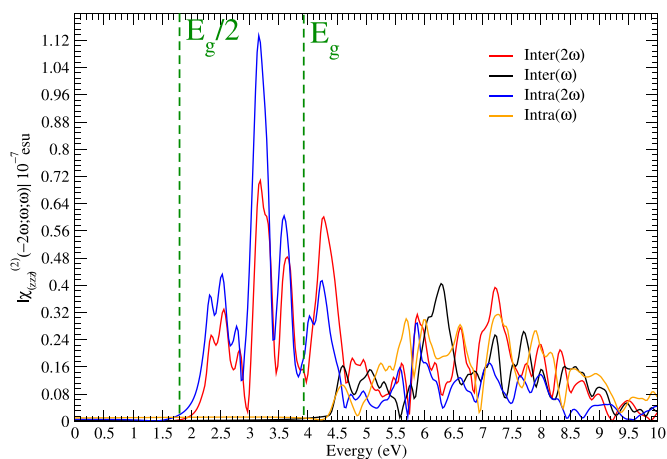


Fig. 8. Intra- $2\omega/\omega$ - and inter- $2\omega/\omega$ -band contributions of the absolute value of the $\chi_{zzz}^{(2)}(2\omega, \omega, \omega)$ component.

response is expected, and this trend is shown from Fig. 7(b), where opposite symmetrical patterns for the ω - and 2ω -resonances occur at higher energies. The typical SHG susceptibility at $\lambda_f = 1064$ nm is found equal to $d_{33} = \chi_{zzz}^{(2)}/2 = 1.38$ pm/V in agreement with the calculated ones of 1.44 pm/V [34] and ~ 2 pm/V [69] for the $\text{CaBi}_2\text{B}_2\text{O}_7$ and $\text{ZnBi}_2\text{B}_2\text{O}_7$ materials, respectively.

4. Conclusion

Herein, a theoretical study is carried out, including both ab initio DFT calculations and analysis based on the topology of electron densities. Our endeavor presents a first tentative to analyze electronic, bonding and optical properties of the $\text{SrBi}_2\text{B}_2\text{O}_7$ single crystal. The structural parameters are found in agreement with the experimental ones. The calculated elastic components affirm the mechanical stability of the investigated compound in its hexagonal structure. Further examination of mechanical properties, like Young modulus and its related properties, indicates brittle behavior of the investigated material. In addition, band structure calculation suggests that the title compound has a wide indirect band gap. This allows us to stipulate that $\text{SrBi}_2\text{B}_2\text{O}_7$ should have much desired high laser damage thresholds relative to the commercial NLO oxides. Several interesting mappings between atoms and polyhedra were revealed by means of the topological analysis of the charge density. As pointed below, the distortion is caused by the stereochemically active lone pair of p/s -cation (Bi^{3+}) which is one of the noticeable factors responsible for the enhancement of the octahedral distortion in the $\text{SrBi}_2\text{B}_2\text{O}_7$ compound. This distortion enhances the local dipole moments, which increase the overall electric susceptibility. The prediction of the absorption spectrum showed that the crystal exhibits high transparency in the UV portion of the spectrum. Moreover, the calculation of the birefringence suggests that the $\text{SrBi}_2\text{B}_2\text{O}_7$ is a negative uniaxial optical crystal; this permitted us to examine the phase matching condition for the SHG process, which makes the $\text{SrBi}_2\text{B}_2\text{O}_7$ single crystal as a good nonlinear material. In addition to its interesting optical properties, the SHG efficiency in the $\text{SrBi}_2\text{B}_2\text{O}_7$ single crystal can be attributed to the synergistic effect between the polarization and the alignment of the multiple $\text{SrO}_6/\text{BiO}_3$ irregular octahedra, as well as, due to the stereochemical activity of the Bi^{3+} multiple lone-pair electrons. Moreover, we studied the nonlinear optical properties of the title material. According to our results, the dominant second order susceptibility component is d_{33} with the largest value of ~ 3.6 times that of KDP, which makes $\text{SrBi}_2\text{B}_2\text{O}_7$ very promising as UV NLO material. The

$\text{SrBi}_2\text{B}_2\text{O}_7$ can be used to absorb light sources below 200 nm. This kind of material is in great demand for various industrial and medical applications, such as microlithographic applications and refractive eye surgery. Solid-state lasers based on frequency conversion in the $\text{SrBi}_2\text{B}_2\text{O}_7$ can generate narrow-band, high-repetition-rate deep-UV light with short pulse duration and have (potentially) longer lifetimes and lower operating costs than excimer lasers.

Acknowledgement

We thank the MALTA Consolider Team and Departamento de Química Física y Analítica, Universidad de Oviedo (Spain), especially Professor J.M. Recio, for giving us access to the computational facilities.

References

- [1] C.T. Chen, Y.C. Wu, R.K. Li, The relationship between the structural type of anionic group and SHG effect in boron-oxygen compounds, *Chin. Phys. Lett.* 2 (1985) 389–392. <https://doi.org/10.1088/0256-307X/2/9/002>.
- [2] C.T. Chen, Y.C. Wu, A.D. Jiang, B.C. Wu, G.M. You, R.K. Li, S.J. Lin, New nonlinear-optical crystal LiB_3O_5 , *J. Opt. Soc. Am.* 6 (1989) 616–621. https://doi.org/10.2184/lsj.19.10_941.
- [3] C. Chen, T. Sasaki, R. Li, Y. Wu, Z. Lin, Y. Mori, Z. Hu, J. Wang, S. Uda, M. Yoshimura, et al., *Nonlinear Optical Borate Crystals*, Wiley-VCH Verlag GmbH & Co. KGaA, Weinheim, Germany, 2012.
- [4] C.T. Chen, B.C. Wu, A.D. Jiang, G.M. You, A new ultraviolet SHG crystal β - BaB_2O_4 , *Sci. Sin.* 18 (1985) 235–243. https://jglobal.jst.go.jp/en/detail?JGLOBAL_ID=200902013841617750&rel=0.
- [5] C. Chen, Y. Wang, B. Wu, K. Wu, Design and synthesis of an ultraviolet-transparent nonlinear optical crystal $\text{Sr}_2\text{Be}_2\text{B}_2\text{O}_7$, *Nature* 373 (1995) 322. <https://www.nature.com/articles/373322a0>.
- [6] Y. Mori, I. Kuroda, S. Nakajima, T. Sasaki, S. Nakai, Nonlinear optical properties of cesium lithium borate, *Jpn. J. Appl. Phys.* 34 (1995) L296–L298. <https://doi.org/10.1143/JJAP.34.L296>.
- [7] Z.G. Hu, T. Higashiyama, M. Yoshimura, Y.K. Yap, Y. Mori, T. Sasaki, A new nonlinear optical borate crystal $\text{K}_2\text{Al}_2\text{B}_2\text{O}_7$ (KAB), *Jpn. J. Appl. Phys.* 37 (1998) L1093–L1094. <https://doi.org/10.1143/JJAP.37.L1093>.
- [8] N. Ye, W.R. Zeng, J. Jiang, B.C. Wu, C.T. Chen, B.H. Feng, X.L. Zhang, New nonlinear optical crystal $\text{K}_2\text{Al}_2\text{B}_2\text{O}_7$, *J. Opt. Soc. Am.* 17 (2000) 764–768. <https://doi.org/10.1364/JOSAB.17.000764>.
- [9] H. Hellwig, J. Liebertz, L. Bohaty, Exceptional large nonlinear optical coefficients in the monoclinic bismuth borate BiB_3O_6 (BIBO), *Solid State Commun.* 109 (1999) 249–251. [https://doi.org/10.1016/S0038-1098\(98\)00538-9](https://doi.org/10.1016/S0038-1098(98)00538-9).
- [10] J. Barbier, N. Penin, A. Denoyer, L.M. Cranswick, BaBiO_4 , a novel non-centrosymmetric borate oxide, *Solid State Sci.* 7 (2005) 10551061. <https://doi.org/10.1016/j.solidstatesciences.2004.11.031>.
- [11] C. Chen, T. Sasaki, R. Li, Y. Wu, Z. Lin, Y. Mori, Z. Hu, J. Wang, S. Uda, M. Yoshimura, et al., *Nonlinear Optical Borate Crystals*, Wiley-VCH Verlag GmbH & Co. KGaA, Weinheim, Germany, 2012.
- [12] V.V. Atuchin, A.K. Subanakov, A.S. Aleksandrovsky, B.G. Bazarov, J.G. Bazarova, S.G. Dorzhieva, T.A. Gavrilova, A.S. Krylov, M.S. Molokeev, A.S. Oreshonkov, A.M. Pugachev, Yu.L. Tushinova, A.P. Yelissev, Exploration of structural, thermal, vibrational and spectroscopic properties of new non-centrosymmetric double borate $\text{Rb}_3\text{NdB}_6\text{O}_{12}$, *Adv. Powder Technol.* 28 (5) (2017) 1309–1315. <https://doi.org/10.1016/j.apt.2017.02.019>.
- [13] V.V. Atuchin, A.K. Subanakov, A.S. Aleksandrovsky, B.G. Bazarov, J.G. Bazarova, T.A. Gavrilova, A.S. Krylov, M.S. Molokeev, A.S. Oreshonkov, S.Yu. Stefanovich, Structural and spectroscopic properties of new noncentrosymmetric self-activated borate $\text{Rb}_3\text{EuB}_6\text{O}_{12}$ with B_5O_{10} units, *Mater. Des.* 140 (2018) 488–494. <https://doi.org/10.1016/j.matdes.2017.12.004>.
- [14] A.B. Kuznetsov, D.M. Ezhov, K.A. Kokh, N.G. Kononova, V.S. Shevchenko, B. Uralbekov, A. Bolatov, V.A. Svetlichnyi, I.N. Lapin, E.A. Simonova, A.E. Kokh, Nonlinear optical crystals $\text{K}_7\text{CaR}_2(\text{B}_5\text{O}_{10})_3$ ($\text{R}=\text{Nd, Yb}$), growth and properties, *J. Cryst. Growth* 519 (2019) 54–59. <https://doi.org/10.1016/j.jcrysgro.2019.05.007>.
- [15] V.V. Atuchin, T. Hasanov, V.G. Kesler, A.E. Kokh, L.D. Pokrovsky, Amorphization and chemical modification of β - BaB_2O_4 surface by polishing, *Opt. Mater.* 23 (1–2) (2003) 385–392. [https://doi.org/10.1016/S0925-3467\(02\)00323-3](https://doi.org/10.1016/S0925-3467(02)00323-3).
- [16] V.V. Atuchin, S.V. Adichtchev, B.G. Bazarov, Zh.G. Bazarova, T.A. Gavrilova, V.G. Grossman, V.G. Kesler, G.S. Meng, Z.S. Lin, N.V. Surovtsev, Electronic structure and vibrational properties of $\text{KRbAl}_2\text{B}_2\text{O}_7$, *Mater. Res. Bull.* 48 (3) (2013) 929–934. <https://doi.org/10.1016/j.materresbull.2012.10.055>.
- [17] V.V. Atuchin, V.G. Kesler, A.I. Zaitsev, M.S. Molokeev, A.S. Aleksandrovsky, A.A. Kuzubov, N.Y. Ignatova, Electronic structure of α - SrB_4O_7 : experiment and theory, *J. Phys. Condens. Matter* 25 (8) (2013) 085503. <https://doi.org/10.1088/0953-8984/25/8/085503>.
- [18] C. Chen, Y. Wu, R. Li, The anionic group theory of the non-linear optical effect

- and its applications in the development of new high-quality NLO crystals in the borate series, *Int. Rev. Phys. Chem.* 8 (1989) 65–91. <https://doi.org/10.1080/01442358909353223>.
- [19] D.N. Nikogosyan, *Nonlinear Optical Crystals: A Complete Survey*, Springer, New York, NY, USA, 1999.
- [20] P. Becker, Borate materials in nonlinear optics, *Adv. Mater.* 10 (1998) 979–992. [https://doi.org/10.1002/\(SICI\)1521-4095\(199809\)10:13<979::AID-ADMA979>3.0.CO;2-N](https://doi.org/10.1002/(SICI)1521-4095(199809)10:13<979::AID-ADMA979>3.0.CO;2-N).
- [21] S. Sen, Atomic environment of high-field strength Nd and Al cations as dopants and major components in silicate glasses: a Nd LIII-edge and Al K-edge X-ray absorption spectroscopic study, *J. Non-Cryst. Solids* 261 (2000) 226. [https://doi.org/10.1016/S0022-3093\(99\)00564-5](https://doi.org/10.1016/S0022-3093(99)00564-5).
- [22] T. Inoue, X. Gao, K. Shinozaki, T. Honma, T. Komatsu, Laser patterning of nonlinear optical $\text{Bi}_2\text{ZnB}_2\text{O}_7$ crystal lines in glass, *Front. Mater.* 2 (2015) 42. <https://doi.org/10.3389/fmats.2015.00042>.
- [23] B. Shanmugavelu, V.V.R.K. Kumar, Crystallization kinetics and phase transformation of bismuth zinc borate glass, *J. Am. Ceram. Soc.* 95 (2012), 2891–1898. <https://doi.org/10.1111/j.1551-2916.2012.05342.x>.
- [24] K. Majhi, K.B. R Varma, Structural, dielectric and optical properties of $\text{CaBi}_2\text{B}_2\text{O}_7$ glasses and glass-nanocrystal composites, *Mater. Chem. Phys.* 117 (2008) 494–499. <https://doi.org/10.1016/j.matchemphys.2009.06.044>.
- [25] K. Majhi, K.B.R. Varma, Structural, dielectric and optical properties of transparent glasses and glass-ceramics of $\text{SrBi}_2\text{B}_2\text{O}_7$, *J. Non-Cryst. Solids* 354 (2008) 4543–4549. <https://doi.org/10.1016/j.jnoncrysol.2008.06.010>.
- [26] V.P. Singh, H.S. Kushwaha, R. Vaish, Photocatalytic study on $\text{SrBi}_2\text{B}_2\text{O}_7$ ($\text{SrO-Bi}_2\text{O}_3\text{-B}_2\text{O}_3$) transparent glass ceramics, *Mater. Res. Bull.* 99 (2018) 453–459. <https://doi.org/10.1016/j.materresbull.2017.11.043>.
- [27] L. Wu, Y. Bai, L. Wu, H. Yi, Y. Kong, Y. Zhang, J. Xu, Sm^{3+} and Eu^{3+} co-doped $\text{SrBi}_2\text{B}_2\text{O}_7$: a red-emitting phosphor with improved thermal stability, *RSC Adv.* 7 (2017) 1146. <https://doi.org/10.1039/C6RA26752A>.
- [28] Z. Li, Q. Pian, L. Li, Y. Sun, S. Zheng, Luminescence properties of $\text{SrBi}_2\text{B}_2\text{O}_7$: Eu^{3+} orange-red phosphor, *Optik* 161 (2018) 38–43. <https://doi.org/10.1016/j.jlloe.2018.01.132>.
- [29] R.S. Bubnova, A.P. Shablinskii, S.N. Volkov, S.K. Filatov, M.G. Krzhizhanovskaya, V.L. Ugolkov, Crystal structures and thermal expansion of $\text{Sr}_{1-x}\text{Ba}_x\text{Bi}_2\text{B}_2\text{O}_7$ solid solutions, *Glass Phys. Chem.* 42 (2016) 337–348. <https://link.springer.com/article/10.1134/S1087659616040040>.
- [30] R.S. Bubnova, S.K. Filatov, High-temperature borate crystal chemistry, *Z. Kristallogr.* 228 (2013) 395–428. <https://doi.org/10.1524/zkri.2013.1646>.
- [31] E.O. Chi, K.M. Ok, Y. Porter, P.S. Halasyamani, $\text{Na}_2\text{Te}_3\text{Mo}_3\text{O}_{16}$: a new molybdenum tellurite with second-harmonic generating and pyroelectric properties, *Chem. Mater.* 18 (2006) 2070–2074. <https://doi.org/10.1021/cm052614e>.
- [32] H. Ra, K.M. Ok, P.S. Halasyamani, Combining second-order JahnTeller distorted cations to create highly efficient SHG materials: synthesis, characterization, and NLO properties of BaTeM_2O_9 ($\text{M} = \text{Mo}^{6+}$ or W^{6+}), *J. Am. Chem. Soc.* 125 (2003) 7764–7765. <https://doi.org/10.1021/ja035314b>.
- [33] R.E. Sykora, K.M. Ok, P.S. Halasyamani, T.E. Albrecht-Schmitt, Structural modification of molybdenyl iodate architectures by alkali metal cations in $\text{AMoO}_3(\text{IO}_3)$ ($\text{A} = \text{K}, \text{Rb}, \text{Cs}$): a facile route to new polar materials with large SHG responses, *J. Am. Chem. Soc.* 124 (2002) 1951–1957. <https://doi.org/10.1021/ja012190z>.
- [34] I. Merad Boudia, A.H. Reshak, T. Ouahrani, Z. Bentalha, Density functional theory calculation of the optical properties and topological analysis of the electron density of $\text{MBi}_2\text{B}_2\text{O}_7$ ($\text{M} = \text{Ca}, \text{Zn}$) compounds, *J. Appl. Phys.* 113 (2013), 083505. <https://doi.org/10.1063/1.4792733>.
- [35] R.F.W. Bader, *Atoms in Molecules, A Quantum Theory*, Oxford University Press, Oxford, 1990.
- [36] F. Tran, P. Blaha, Accurate band gaps of semiconductors and insulators with a semilocal exchange-correlation potential, *Phys. Rev. Lett.* 102 (2009) 226401. <https://doi.org/10.1103/PhysRevLett.102.226401>.
- [37] J. Srour, M. Badawi, F.E.H. Hassan, A.V. Postnikov, Crystal structure and energy bands of $(\text{Ga}/\text{In})\text{Se}$ and $\text{Cu}(\text{In}, \text{Ga})\text{Se}_2$ semiconductors in comparison, *Phys. Status Solidi B* 253 (8) (2016) 1472–1475. <https://doi.org/10.1002/pssb.201552776>.
- [38] J. Srour, M. Badawi, F. El Haj Hassan, A. Postnikov, Comparative study of structural and electronic properties of GaSe and InSe polytypes, *J. Chem. Phys.* 149 (5) (2018), 054106. <https://doi.org/10.1063/1.5030539>.
- [39] <http://elk.sourceforge.net/>.
- [40] J.R. Perdew, Y. Wang, Accurate and simple analytic representation of the electron-gas correlation energy, *Phys. Rev. B Condens. Matter* 45 (1992) 13244–13249. <https://doi.org/10.1103/PhysRevB.45.13244>.
- [41] J.P. Perdew, K. Burke, M. Ernzerhof, Generalized gradient approximation made Simple, *Phys. Rev. Lett.* 77 (1996) 3865. <https://doi.org/10.1103/PhysRevLett.77.3865>.
- [42] E. Engel, S.H. Vosko, Exact exchange-only potentials and the virial relation as microscopic criteria for generalized gradient approximations, *Phys. Rev. B* 47 (1993) 13164. <https://doi.org/10.1103/PhysRevB.47.13164>.
- [43] C. Ambrosch-Draxl, J.O. Sofo, Linear optical properties of solids within the full-potential linearized augmented planewave method e-print arXiv: cond-mat/0402523.
- [44] T. Ouahrani, Otero-de-la-Roza, M. Mebrouki, V. Luaña, R. Khenata, B. Amrani, First-principles study of structural, electronic, linear and nonlinear optical properties of Ga_2PbSb ternary chalcocopyrite, *Eur Phys J B* 72 (2009) 361. <https://doi.org/10.1140/epjpb/e2009-00345-6>.
- [45] A.D. Becke, K.E. Edgecombe, A simple measure of electron localization in atomic and molecular systems, *J. Chem. Phys.* 92 (1990) 5397. <https://doi.org/10.1063/1.458517>.
- [46] A. Otero-de-la-Roza, E.R. Johnson, V. Luaña, CRITIC2: a program for real-space analysis of quantum chemical interactions in solids, *Comput. Phys. Commun.* 185 (2014) 1007–1018. <https://doi.org/10.1016/j.cpc.2013.10.026>.
- [47] T. Ouahrani, Chemical and physical insight on the local properties of the phosphides XSIP_2 ($\text{X} = \text{Be}, \text{Mg}, \text{Cd}, \text{Zn}$ and Hg) under pressure: from first principles calculations, *Eur Phys J B* 86 (9) (2013) 369. <https://doi.org/10.1016/j.cpc.2013.10.026>.
- [48] J. Barbier, L.M.D. Cranswick, The non-centrosymmetric borate oxides, $\text{MBi}_2\text{B}_2\text{O}_7$ ($\text{M} = \text{Ca}, \text{Sr}$), *J. Solid State Chem.* 179 (2006) 3958–3964. <https://doi.org/10.1016/j.jssc.2006.08.037>.
- [49] A. Jain, S.P. Ong, G. Hautier, W. Chen, W.D. Richards, S. Dacek, S. Cholia, D. Gunter, D. Skinner, G. Ceder, K.A. Persson, The Materials Project: a materials genome approach to accelerating materials innovation, *Apl. Mater.* 1 (1) (2013), 011002. <https://doi.org/10.1063/1.4812323> <https://doi.org/10.1063/1.4812323>.
- [50] Y. Le Page, P. Saxe, Symmetry-general least-squares extraction of elastic data for strained materials from ab initio calculations of stress, *Phys. Rev. B* 65 (2002) 104104. <https://doi.org/10.1103/PhysRevB.65.104104>.
- [51] R. Hill, The elastic behaviour of a crystalline aggregate, *Phys. Soc. Lond. Sect. A* 65 (1952) 349–354. <https://doi.org/10.1088/0370-1298/65/5/307>.
- [52] X. Zhang, W. Huang, H. Ma, H. Yu, W. Jiang, First-principles prediction of the physical properties of $\text{ThM}_2\text{Al}_2\text{O}$ ($\text{M} = \text{Ti}, \text{V}, \text{Cr}$) intermetallics, *Solid State Commun.* 284–286 (2018) 75–83. <https://doi.org/10.1016/j.ssc.2018.09.008>.
- [53] S. Zhu, X. Zhang, J. Chen, C. Liu, F. Wang, Insight into the elastic, electronic properties, anisotropy in elasticity of Manganese Borides, *Vacuum* 165 (2019) 118–126. <https://doi.org/10.1016/j.vacuum.2019.04.014>.
- [54] X. Zhang, W. Huang, J. Chen, C. Liu, W. Jiang, Phase stability, elastic, anisotropic and thermodynamic properties of $\text{GdT}_2\text{Al}_2\text{O}$ ($\text{T} = \text{Ti}, \text{V}, \text{Cr}$) compounds: a first-principles study, *Vacuum* 157 (2018) 312–319. <https://doi.org/10.1016/j.vacuum.2018.09.001>.
- [55] Y. Lv, X. Zhang, W. Jiang, Phase stability, elastic, anisotropic properties, lattice dynamical and thermodynamic properties of B_1M ($\text{M} = \text{Th}, \text{U}, \text{Np}, \text{Pu}$) dodecaborides, *Ceram. Int.* 44 (2018) 128–135. <https://doi.org/10.1016/j.ceramint.2017.09.147>.
- [56] X. Zhang, J. Chen, F. Wang, X. Chen, H. Ma, D. zhiLi, C. Liu, H. Guod, Insight into the elastic and anisotropic properties of BiMg_2MO_6 ($\text{M} = \text{P}, \text{as}$ and V) ceramics from the first-principles calculations, *Ceram. Int.* 45 (2019) 11136–11140. <https://doi.org/10.1016/j.ceramint.2017.09.147>.
- [57] G. Kresse, D. Joubert, From ultrasoft pseudopotentials to the projector augmented-wave method, *Phys. Rev. B* 59 (1999) 1758–1775. <https://doi.org/10.1103/PhysRevB.59.1758>.
- [58] P. Mori-Sánchez, A. Martín Pendás, V. Luaña, A classification of covalent, ionic, and metallic solids based on the electron density, *J. Am. Chem. Soc.* 124 (2002) 14721. <https://doi.org/10.1021/ja027707t>.
- [59] L. Li, Y. Wang, B.H. Lei, S. Han, Z. Yang, K.R. Poeppelmeier, S. Pan, A new deep-ultraviolet transparent orthophosphate LiCs_2PO_4 with large second harmonic generation response, *J. Am. Chem. Soc.* 138 (2016) 9101–9104. <https://doi.org/10.1021/jacs.6b06053>.
- [60] C.T. Chen, in: V.S. Letokhov, C.V. Shank, Y.R. Shen, H. Walther Harwood (Eds.), *Development of New Nonlinear Optical Crystals in the Borate Series*, Academic, Chur, 1993.
- [61] R. Mahiaoui, T. Ouahrani, A. Chikhaoui, A. Morales-García, A.H. Reshak, Electronic, bonding, linear, and nonlinear optical properties of $\text{Na}_2\text{MGe}_2\text{Q}_6$ ($\text{M} = \text{Cd}, \text{Zn}, \text{Hg}$; $\text{Q} = \text{S}, \text{Se}$), $\text{Na}_2\text{ZnSi}_2\text{S}_3$, and $\text{Na}_2\text{ZnSn}_2\text{S}_3$ two metal-mixed chalcogenide compounds: insights from an ab initio study, *J. Phys. Chem. Solids* 119 (2018) 220–227. <https://doi.org/10.1016/j.jpccs.2018.04.003>.
- [62] O. Mebkhou, T. Ouahrani, A. Morales-García, B. Lasri, J. Pilme, A.H. Reshak, From micro-to macroscopic: understanding optical properties in zinc-blend-derived materials Cu_2ZnYX_2 ($\text{X} = \text{S}, \text{Se}, \text{Tl}, \text{Y} = \text{Si}, \text{Ge}, \text{Sn}$) by means of the quantum chemical topology analysis, *J. Alloy. Comp.* 653 (2015) 140–147. <https://doi.org/10.1016/j.jallcom.2015.08.270>.
- [63] O. Azzi, F. Boukli Hacene, A.K. Ferouani, T. Ouahrani, A.H. Reshak, Electronic, bonding and optical properties of the $\text{LiGaGe}_2\text{X}_6$ ($\text{X} = \text{S}, \text{Se}, \text{and Te}$) compounds: an ab initio study, *Optik* 180 (2019) 782791. <https://doi.org/10.1016/j.jlloe.2018.11.127>.
- [64] C. Chen, T. Sasaki, R. Li, Y. Wu, Z. Lin, Y. Mori, Z. Hu, J. Wang, S. Uda, M. Yoshimura, Y. Kaneda, *Nonlinear Optical Borate Crystals*, vol. 12, Wiley-VCH Verlag & Co. KGaA, Boschstr Weinheim, Germany, 2012, p. 69469.
- [65] J. Lin, M.-H. Lee, Z.-P. Liu, C.C. Chris, J. Pickard, Mechanism for linear and nonlinear optical effects in $\beta\text{-BaB}_2\text{O}_4$ crystals, *Phys. Rev. B* 60 (19) (1999) 15. <https://doi.org/10.1063/1.1533734>.
- [66] W. Zhang, H. Yu, H. Wu, P.S. Halasyamani, Phase-Matching in nonlinear optical compounds: a materials perspective, *Chem. Mater.* 29 (2017) 2655–2668. <https://doi.org/10.1021/acs.chemmater.7b00243>.
- [67] D.A. Kleinman, Nonlinear dielectric polarization in optical media, *Phys. Rev.*

- 126 (1962) 1977–1979, <https://doi.org/10.1103/PhysRev.126.1977>.
- [68] A. Authier, *International Tables for Crystallography*, kluwer academic publishers dordrecht/boston/london, 2003.
- [69] A.H. Reshak, X. Chen, I.V. Kityk, S. Auluck, Specific features of second order optical susceptibilities for a complex borate crystal $\text{Bi}_2\text{ZnB}_2\text{O}_7$: experiment and theory, *Curr. Opin. Solid State Mater. Sci.* 11 (2007) 33–39. <https://doi.org/10.1016/j.cossms.2008.06.001>.